

Single-Molecule Dendrimer-Hydrocarbon Interaction

Karthikeyan Pasupathy,^a Nicholas W. Suek,^b John L. Lyons,^b Justin Ching,^c Aaron Jones,^a Qi Lu,^c Monica H. Lamm,^{b,*} and Pu Chun Ke^{a,*}

^a Laboratory of Single-Molecule Biophysics and Polymer Physics, Clemson University, Clemson, SC 29634, USA

^b Department of Chemical and Biological Engineering, Iowa State University, Ames, IA 50011, USA

^c Department of Physics, St. John's University, Queens, NY 11439, USA

Abstract: We report our single-molecule fluorescence microscopy and molecular dynamics simulation studies on the interaction of poly(amidoamine) dendrimer and squalane hydrocarbon in aqueous solution. Our spectrophotometry measurements indicate that this interaction increases with the pH of the solvent. Our simulations show that squalane resides primarily on the perimeter of the dendrimer at low to neutral pH, but becomes encapsulated by the dendrimer at high pH. Using single-molecule fluorescence microscopy, we have identified that the binding between PAMAM and squalane is reversible. At a pH value of 8, the approaching, binding, and characteristic times of a single fluorescently-labeled dendrimer to squalane are 0.5 s, 7.5 s, and 0.5 s, respectively. Both our spectrophotometry measurements and simulations show that the interaction between PAMAM and squalane is stronger for lower generation dendrimers. This study facilitates our understanding of using dendritic and hyperbranched polymers for gas hydrate prevention in the petroleum industry.

INTRODUCTION

Dendrimers are a unique class of nonlinear polymers which can be synthesized from a central core to include many branches or generations through repetitive chemistry [1]. Due to their appealing physical and chemical properties such as high homogeneity, low viscosity, radial symmetry, multivalency, and small size, dendrimers have found increasing applications in nanotechnology, supramolecular chemistry, and catalysis [2-7]. In gene and drug delivery, especially, dendrimers at physiological conditions are electrostatically accessible by nucleic acids [8] and their end groups can be functionalized to incorporate fluorescent tags, as well as drug or prodrug loads [1,9,10]. The amphiphilicity and the nanometer size of dendrimers further promote their efficient cellular and tissue transport.

One promising practice regarding the use of dendrimers and other hyper-branched polymers is their effective prevention of gas hydrate formation in the oil pipeline, a problem that plagues the petroleum industry [11-13]. At high pressures and low temperatures, as is the case with oil production and deep-sea transportation, hydrates constantly occur when water hydrogen bonds with the hydrocarbons in gas and oil products. In sufficient quantities these hydrates can completely block pipelines by agglomerating to create very stable, ice-like plugs, leading to disruptive and costly production stoppages [14]. Dendritic polymers can act as anti-agglomerants or "surfactants" by preventing large hydrates from forming and keeping small crystals suspended in the production flow [11]. The major advantages of using den-

dritic polymers are low doses and elimination of a recovery stage as required by conventional reagents including anti-freeze and methanol. However, the underlying mechanisms of dendrimer-hydrocarbon interactions are poorly understood.

The major purpose of this paper is to understand dendrimer-hydrocarbon interaction at the molecular level. We chose intermediate generation-3 poly(amidoamine), or G3-PAMAM, as the model dendrimer. The justifications of using this dendrimer are two fold. First, PAMAM is one of the most commonly synthesized dendrimers. Second, while G1-G10 PAMAM are all commercially available, the binding of low-generation dendrimers and hydrocarbon is stronger than the higher generations as we will demonstrate later. We selected squalane, a natural extract from olive oil, as the model hydrocarbon. We examined the effects of solvent pH on the binding of PAMAM and squalane using spectrophotometry and molecular dynamics simulations. We further characterized the interaction kinetics using single-molecule fluorescence microscopy. In principle our results should be applicable to hyperbranched polymers and dendrimers of other generations.

METHODS

(a) Spectrophotometry

Pure squalane (Supelco, C₃₀H₆₂, MW 422, Fig. (1A)) was vortexed with G1, G3, or G5-PAMAM (Dendritech) of equal concentration (0.45 mM). The final concentration of the squalane was estimated to be 0.96 mM. For generation dependence, the absorption spectra of the mixtures (pH = 8, each stabilized for 10 min) were acquired using a Biomate 3 spectrophotometer. For pH dependence, the absorption spectra were measured for G3-PAMAM-squalane mixtures of pH 2, 8, and 10 adjusted using Fluka buffers (SB series, Fisher). The temperature dependence of G3-PAMAM and squalane

*Address correspondence to these authors at the Laboratory of Single-Molecule Biophysics and Polymer Physics, Clemson University, Clemson, SC 29634, USA; Tel: 864-656-0558; Fax: 864-656-0805; E-mail: pcke11@clemson.edu; the Department of Chemical and Biological Engineering, Iowa State University, Ames, IA 50011, USA; Tel: 515-294-6533; Fax: 515-294-2689; E-mail: mhlamm@iastate.edu

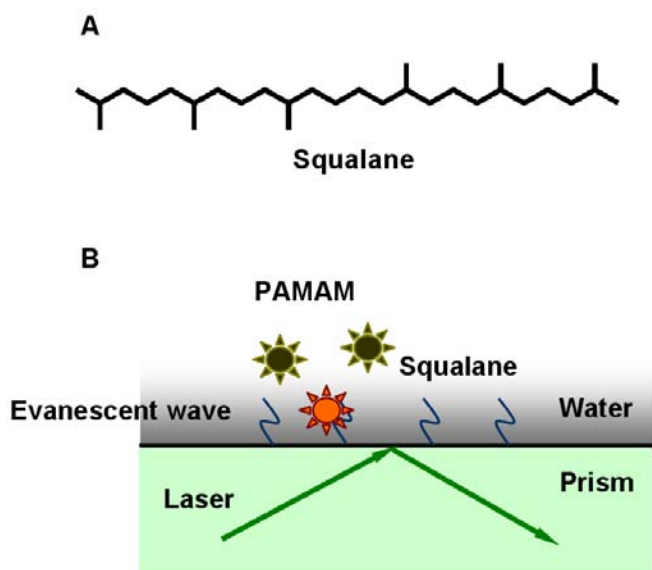


Fig. (1). (A) Structure of a squalane molecule. (B) Scheme of the TIR fluorescence microscopy setup for measuring the binding between PAMAM (in water) and squalane (immobilized on a glass slide attached to a prism via immersion oil). The incidence angle of the laser beam satisfies TIR condition to produce an evanescent wave above the prism surface. PAMAM emits fluorescence (orange) when it enters the evanescent wave generated by the laser beam, otherwise remains nonfluorescent (dark green).

interaction was measured using a Cary 300 BIO spectrophotometer with temperature adjusted from 15–23°C at an increment of 2°C and a time interval of 3 min.

(b) Labeling Dendrimers

G3-PAMAM was labeled using 5(6)-TRITC (Anaspec, $\lambda_{\text{ex}} = 543 \text{ nm}$, $\lambda_{\text{em}} = 571 \text{ nm}$) at a 1:2 molar ratio and incubated in darkness overnight. This labeling ratio allowed 2 out of the 32 primary amines of each PAMAM molecule to react with the isothiocyanate group of the TRITC. This low labeling ratio also ensured minimal structural and chemical alterations to the primary amines of the PAMAM. The un-reacted TRITC was filtered out using Microcon YM-3 filters (Millipore, MWCO 3,000 Da). The concentration of the filtered solution was estimated to be 0.18 mM using spectrophotometry.

(c) Single-Molecule Total-Internal-Reflection Fluorescence Microscopy

A microscope glass slide was sonicated in 2% Micro-90 solution, washed thoroughly with Milli-Q water, and dried at 400°C for 4 hr in a kiln. A squalane solution of 10 μL (0.19 mM, in acetone) was coated onto the clean glass slide at 500 rpm for 3 s and 6,000 rpm for 60 s consecutively using a spin coater (WS-400B Laurell Technologies). Topological imaging using an atomic force microscope (Veeco Dimension 3100) confirmed that the thickness of the thin film was less than 50 nm.

A total-internal-reflection (TIR) fluorescence microscope was used for imaging the interaction between single TRITC-labeled G3-PAMAM in aqueous solution and squalane im-

mobilized on the glass slide to simulate the phase separations between the amphiphilic dendrimer and the hydrophobic hydrocarbon (Fig. (1B)). The TIR condition was obtained using a frequency-doubled Nd⁺:YAG laser (CystaLaser, $\lambda = 532 \text{ nm}$) at a larger than the critical incidence angle and a dove prism (OptoSigma). A sample cell was formed by double-sided tapes sandwiched between the glass slide and a cover glass. The slide was attached to the prism via refractive-index matching immersion oil. Immediately prior to imaging, 10 μL of TRITC-labeled G3-PAMAM (13 nM, pH = 8) was flowed in the sample cell. The pH value was chosen to mimic the conditions in an oil pipeline. When a PAMAM molecule diffused into the evanescent wave generated by the laser beam, i.e., within $\sim 100 \text{ nm}$ from the slide surface [15], the molecule was excited and its fluorescence shown as a bright spot in the image. Conversely, no fluorescence was excited when the molecule diffused out of the evanescent field. In the experiment the fluorescence of PAMAM was captured using a CCD camera with single-photon counting sensitivity (Roper Scientific, 512B). Over 650 data sets were acquired using WinView32 and analyzed using the MATLAB program developed in our lab. Each of the data set contained 600 image frames with an exposure of 0.2 sec/frame. The time-lapse intensities of the fluorescence spots in each image were tracked and counted against background noise. Three characteristic times, T_1 , T_2 , and T_3 (cf. Fig. (7) inset, derived from average fluorescence intensities registered on a CCD camera), were obtained and their histograms were plotted and fit with Gaussian curves in Origin and Excel.

(d) Molecular Dynamics Simulation

All molecular dynamics simulations were performed in aqueous solution using LAMMPS (Large-scale Atomic/Molecular Massively Parallel Simulator) [16]. The Dreiding force field [17] was used for PAMAM and squalane, while the TIP3P force field [18] was used for water. To model pH effects, we protonated the amines in the dendrimer according to the scheme used in [19, 20]: i.) high pH (> 10), no protonation; ii.) medium or neutral pH (~ 7), all primary amines are protonated; iii.) low pH (< 4), all primary and tertiary amines are protonated. The atomic coordinates for the unprotonated G3 and G5-PAMAM dendrimers were obtained from [21]. PyMol was used to protonate the dendrimer to the proper pH level and to add Cl⁻ counterions to maintain charge neutrality. The procedure for building and modeling the aqueous dendrimer-squalane complex at each pH was as follows. The dendrimer (and counterions for neutral and low pH) was placed in a box of water, with at least 10 Å between any atom of the dendrimer and the edge of the simulation box, and equilibrated for 500 ps. The water was removed, a squalane molecule was added to the equilibrated dendrimer structure, and the system was re-solvated with water. The final dendrimer/squalane/water system was then run for 2 ns of molecular dynamics to monitor the interaction between dendrimer and squalane. The radii of gyration for all dendrimer atoms (R_g) and the nitrogen atoms (R_N) in the primary amines were monitored to judge when the system reached equilibrium. A spring force between the center-of-masses of the squalane and dendrimer was used to push the two molecules together for the first 10 ps. The spring force was then turned off for the remainder of the run.

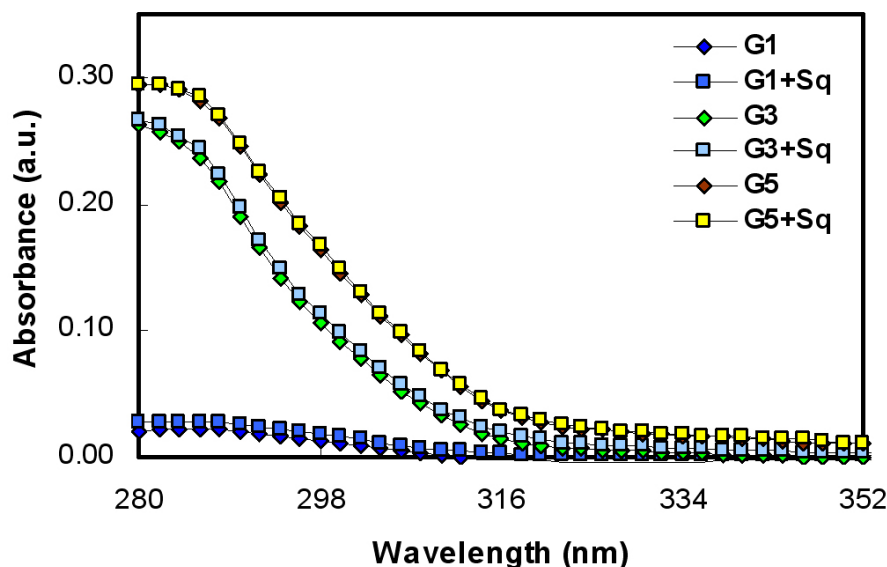


Fig. (2). Dependence of PAMAM-squalane interaction on dendrimer generation. At 280 nm, the absorbance was increased by 28.5%, 2%, and 0% respectively for equal molar of G1, G3, and G5-PAMAM mixed with fixed amount of squalane. The increases of the absorbance were due to the binding of squalane from air-water interfaces to PAMAM in the suspensions. Symbol “Sq” in the figure legend denotes the addition of squalane otherwise it refers to PAMAM of various generations.

All simulations were carried out at 300 K and 1 atm using the Nose-Hoover thermostat and barostat. The equations of motion were integrated with a 1 fs time step. A cutoff of 10 Å was used for van der Waals interactions and the PPPM (particle-particle particle-mesh) solver [22] was used for Coulombic interactions. The radius of gyration, R_g , of the dendrimer was monitored during the simulations to estimate the size of the dendrimer. This quantity is given by

$$\langle R_g^2 \rangle = \langle [\sum_i m_i (r_i - r_{cm})^2] \rangle / M \quad (1)$$

where M is the total mass of the dendrimer, m_i is the mass of atom i , r_i is the position of atom i , and r_{cm} is the center-of-mass of the dendrimer. Another estimate of size is R_N , the radius of gyration considering only the nitrogen atoms in the primary amines.

RESULTS AND DISCUSSION

As shown in Fig. (2), the absorbance of G1, G3, and G5-PAMAM was increased by 28.5%, 2%, and 0%, respectively, after mixed with equal amount of squalane ($\lambda = 280$ nm). These increases were due to the binding of the hydrophobic squalane originally at the air-water interfaces to form complexes with the PAMAM in the suspensions. This measurement suggests the interaction between PAMAM and squalane is greater for dendrimers of lower generations, where surface groups are fewer, branches are shorter (and more rigid), and interiors are more accessible for the squalane to bind. To confirm the generation effect on binding, we conducted molecular dynamics simulations of G1, G3, and G5-PAMAM dendrimers interacting with squalane in an explicit water environment at neutral pH. Fig. (3) shows the instantaneous distance of separation between the centers of mass of PAMAM and squalane, along with R_g and R_N for each generation. Representative snapshots of the complexes, collected after 1 ns, are shown to the right. For

G1, the squalane remains within 6 Å of the dendrimer center of mass and wraps around the surface of the dendrimer. For generations 3 and 5, the squalane is kept further from the center of mass of the dendrimer and is restricted to interacting with the surface of the dendrimer. Based on these observations we focus on G3-PAMAM for the rest of the study.

We have examined temperature effect on the binding of G3-PAMAM and squalane. The temperature of the G3-PAMAM-squalane mixture was adjusted from 15°C to 23°C at an increment of 2°C. To ensure equilibrium, absorbance of the mixture was recorded every 3 min after a new temperature was set. We observed no more than 0.1% fluctuation of the absorbance for all the temperatures, indicating the binding of PAMAM and squalane is temperature insensitive.

The pH dependence of the dendrimer-hydrocarbon interaction has been studied and is shown in Fig. (4), where both the absorbance values of G3-PAMAM and G3-PAMAM-squalane increase monotonically with the pH of the solvent. In particular, with the addition of squalane, the absorbance of the solution at 280 nm was increased by 20%, 8%, and 8% for pH values of 2 (low pH), 8 (medium pH), and 10 (high pH), respectively. These increases are believed to be caused by the association of the squalane with the dendrimer. To test this hypothesis, we conducted molecular dynamics simulations of a G3-PAMAM and squalane in explicit water at high, medium (neutral), and low pH. Fig. (5) shows the instantaneous distance of separation between the centers of mass of the G3-PAMAM and the squalane, along with the radii of gyration of the dendrimer at high and low pH. At high pH (no protonation), the dendrimer encapsulates the squalane after 600 ps. At neutral pH (all primary amines protonated), shown in Fig. (3B), the squalane interacts with the surface of the dendrimer but never penetrates it. At low pH (all primary and tertiary amines protonated), the squalane briefly explores the interior of the dendrimer but spends a significant amount of time near the surface of the

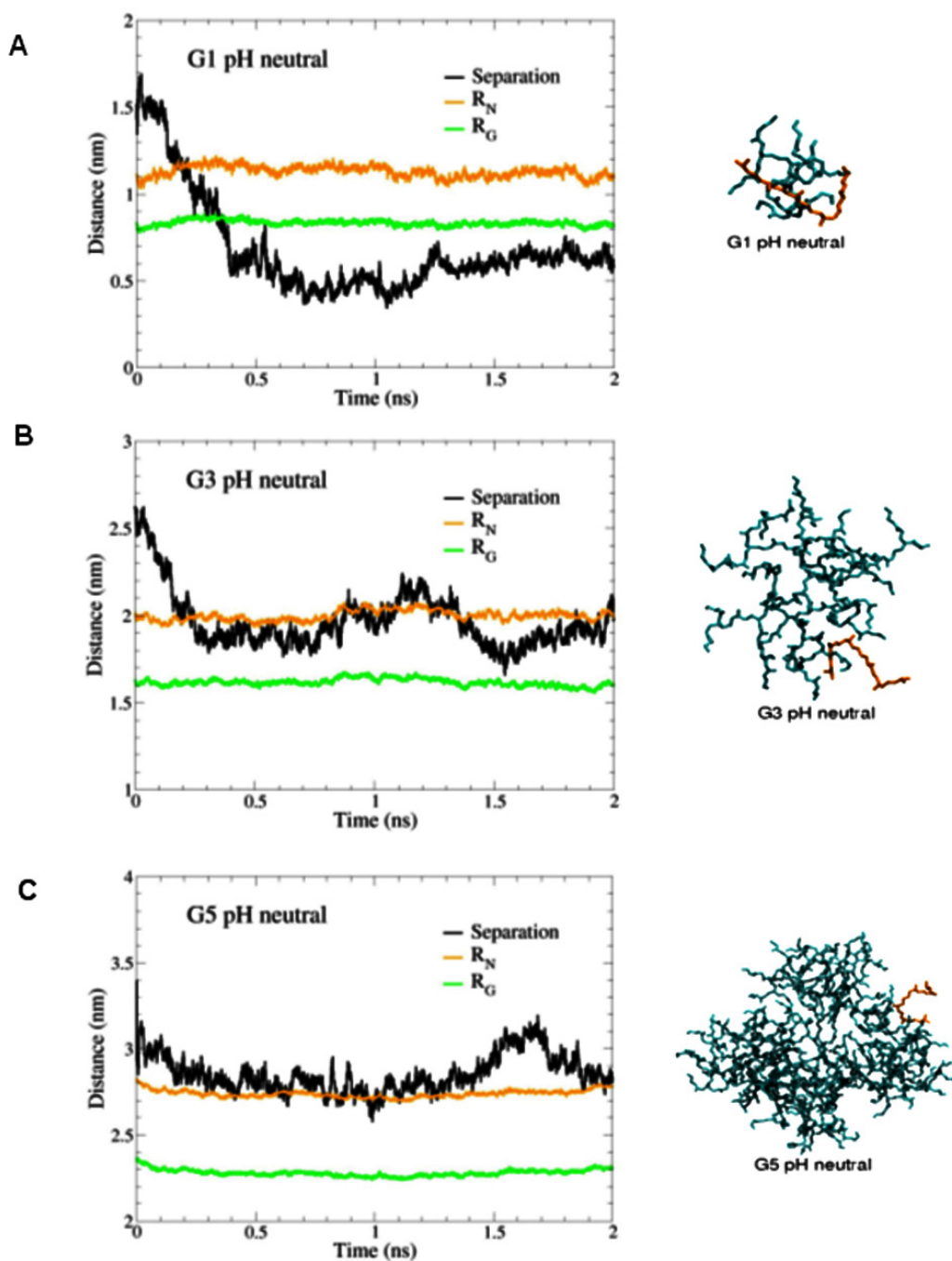


Fig. (3). Distance of separation between the centers of mass of PAMAM and squalane for: (A) G1, (B) G3, and (C) G5. The instantaneous radii of gyration for all dendrimer atoms (R_G) and the nitrogen atoms (R_N) in the primary amines are shown for comparison. Snapshots of the PAMAM (ball-stick) and squalane (orange) complexes from the molecular dynamics simulations are shown to the right. The images for G3 and G5 are not shown to the proper scale relative to G1. On the PAMAM dendrimers, carbon (cyan), nitrogen (blue), and hydrogen (white) atoms are shown. Hydrogen atoms on the squalane, water molecules and counterions have been removed for clarity. The images were rendered using VMD [25].

dendrimer. The fluctuations in the centers of mass separation distance for the neutral and low pH cases are larger than those for the high pH case, indicating that binding interaction at neutral and low pH is weaker.

Representative snapshots of the complexes, collected after 1 ns, are shown to the right in Fig. (5). These images illustrate how the dendrimer conformation changes with de-

creasing pH. The relatively compact structure at high pH provides a favorable hydrophobic environment for squalane, while the more open structures at neutral and low pH (due to electrostatic repulsion between protonated amines) allow more water molecules into the interior and thus, provide a less favorable environment for the squalane. The solvent pH effects on dendrimer size and conformation obtained here are

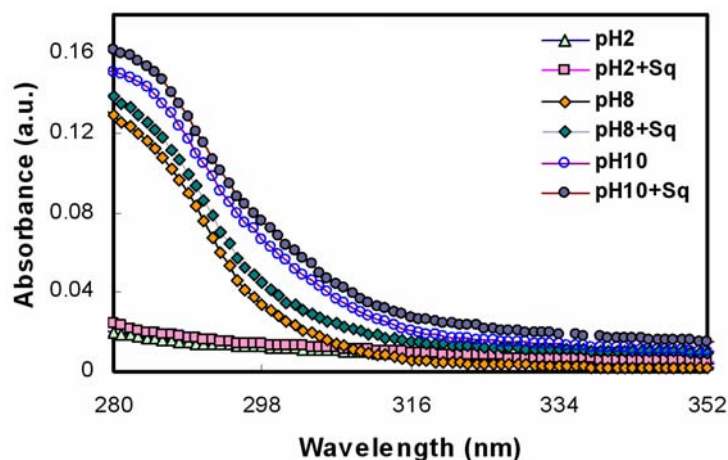
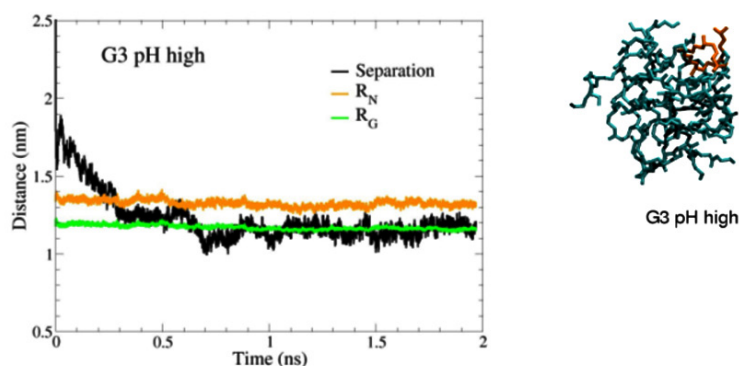


Fig. (4). Measured pH dependence of PAMAM and PAMAM-squalane. The pH value of the water solvent was adjusted to 2, 8, and 10, respectively. Symbol "Sq" in the figure legend denotes the addition of squalane otherwise it refers to PAMAM alone.

A



B

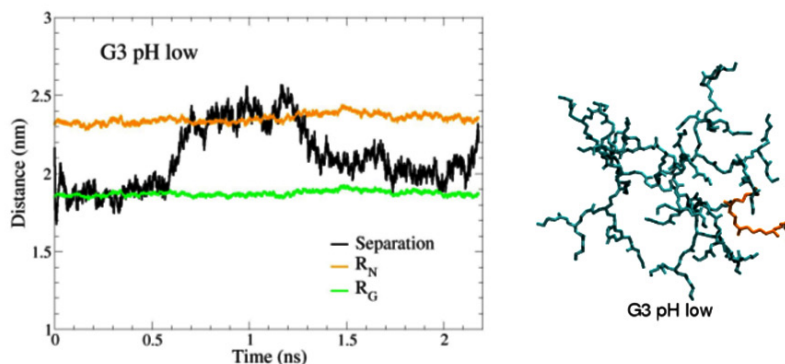


Fig. (5). Distance of separation between the centers of mass of PAMAM and squalane at: (A) high and (B) low pH. The instantaneous radii of gyration for all dendrimer atoms (R_g) and the nitrogen atoms (R_N) in the primary amines are shown for comparison. Snapshots of the G3-PAMAM and squalane complexes from molecular dynamics simulations are shown to the right. See Fig. (3) for color scheme. The neutral pH case for G3-PAMAM is shown in Fig. (3B). Hydrogen atoms, water molecules and counterions have been removed for clarity. The images were rendered using VMD [25].

consistent with previous experimental [23,24,26] and theoretical [20,27-30] characterization of PAMAM in solution.

A comparison between Fig. (6A) (control slide, plain) and B (slide, sparsely coated with squalane) further confirms the interaction between PAMAM and squalane. The number of bright spots, representing single fluorescently-labeled PAMAM molecules entrapped in the evanescent wave by the squalane, is significantly more in Fig. (6B) than in Fig. (6A). In our experiment we also observed the disappearance of

bright spots over time, which is attributed to the dissociation of PAMAM from the squalane.

Our fluorescence imaging further suggests that the binding of PAMAM and squalane is reversible, probably caused by the competition between weak inter- and intramolecular forces and Brownian motion. We describe such a reversible process in three steps: approaching (PAMAM searching for immobilized squalane in the evanescent wave), binding (formation of PAMAM-squalane supramolecular com-

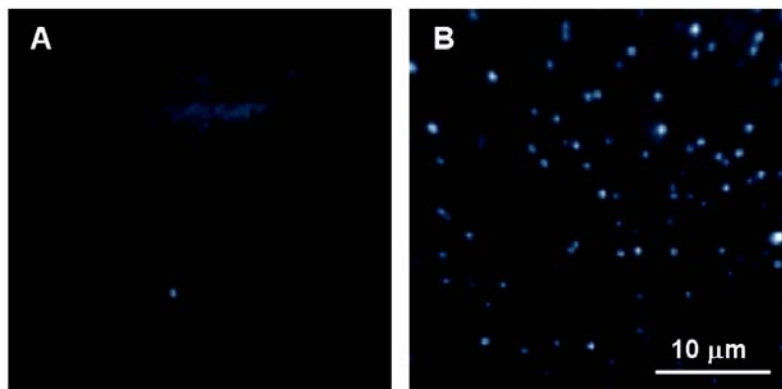


Fig. (6). (A) Fluorescence image of TRITC-labeled PAMAM on a plain glass slide without squalane coating. Very few PAMAM molecules are observed. (B) Fluorescence image of single TRITC-labeled PAMAM molecules (13 nM) adsorbed on a glass slide sparsely coated with squalane. The binding of PAMAM to squalane is evident.

plexes), and dissociation (PAMAM departing from squalane). In other words, when a PAMAM molecule approaches the glass slide through diffusion, the dendrimer may initiate its interaction with a squalane via one or a few branches. This process can be manifested by the approaching characteristic time T_1 (Fig. (7)). When more branches of the PAMAM come in contact with the squalane, or the squalane molecules in proximity, binding characteristic time T_2 takes over till most of the branches of the PAMAM are detached from the hydrocarbon. Opposite to T_1 , the dissociation characteristic time T_3 describes the process when the last branch of the dendrimer is detached till the dendrimer diffuses out of the evanescent wave. In our experiment where the pH value was 8, the averaged characteristic times, T_1 , T_2 , and T_3 , were determined to be 0.5 ± 0.3 s, 7.5 ± 6 s, and 0.5 ± 0.3 s from the Gaussian fitting curves (solid lines, Fig. (7)). Interestingly the values of T_1 and T_3 showed little differences possibly because of the random nature of Brownian motion and the nonspecific interaction between the dendrimer and the hydrocarbon. Based on Figs. (4) and (5), we expect these measured characteristic times, especially T_2 , will change with the pH of the solvent. However, the time scales of such kinetic processes are beyond the capability of our atomistic simulations.

CONCLUSION

We have examined the molecular interactions between dendrimer and hydrocarbon using combined techniques of spectrophotometry, TIR fluorescence microscopy, and atomistic simulations. We have found the interactions between dendrimer and hydrocarbon are temperature insensitive but are dendrimer-generation and solvent-pH dependent. The binding of squalane to PAMAM is stronger for lower generations of dendrimers, possibly due to the more open interiors of the latter for interaction. Regarding the pH effect, at a high pH value of 10, the PAMAM dendrimer is neutral and assumes a small radius of gyration. Such a flexible structure allows for the uptake of squalane hydrocarbon via hydrophobic interaction. At neutral pH, the end groups of the PAMAM become cationic. As a result, the radius of gyration of the PAMAM is increased and the interiors of the dendrimer cater more water molecules to discourage squalane binding. At low pH where all the PAMAM amines are protonated, the dendrimer molecule is swelled and its branches

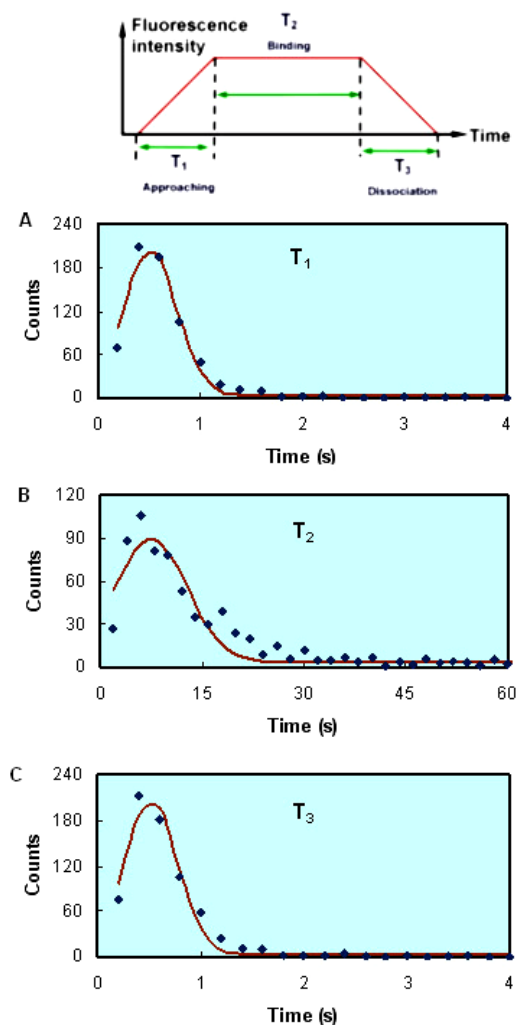


Fig. (7). Measured characteristic times (A) $T_1=0.5 \pm 0.3$ s, (B) $T_2=7.5 \pm 6$ s, and (C) $T_3=0.5 \pm 0.3$ s for approaching, binding, and dissociation of PAMAM with respect to immobilized squalane (pH=8). The numbers after “ \pm ” denote the half widths at half maxima from Gaussian fitting (solid lines in A-C). The characteristic times are defined by the average fluorescence intensities on a CCD camera (top, inset).

become more rigid due to mutual repulsion. Consequently, the interiors of the dendrimer allocate more water to further suppress the attachment of the hydrocarbon.

The interactions between PAMAM and squalane have also been found to be reversible at physiological pH, where weak inter- and intramolecular forces may succumb to Brownian motion. We have further determined the approaching, binding, and dissociation characteristic times as 0.5 s, 7.5 s and 0.5 s, respectively. Since the binding affinity is subject to the total number of squalane molecules in contact with one PAMAM molecule, or vice versa, we believe the time constants, especially the binding characteristic time T_2 , will further increase with the pH of the solvent.

Due to technical limitations our experimental designs and simulations conditions are less hydrophobic than the practical environment of an oil pipeline. However, we believe that our study of dendrimer-hydrocarbon interaction at the molecular level is a major step towards unraveling the mechanisms of gas hydrate prevention. We comprehend that high pH values are favorable for the encapsulation of hydrocarbon or gas molecules by dendrimers or hyper-branched polymers. Such conditions will facilitate the removal of gas hydrate blockages in the oil pipeline. Our study can also be applied to the general case of loading hydrophobic molecules onto branched polymers, such as encapsulating molecules inside a dendrimer for cell trafficking [31,32] and gene delivery [33]. Another extension from this research lies in our fundamental understanding of the diffusion and reptation of nonlinear polymers [34,35].

ACKNOWLEDGEMENTS

PCK acknowledges support from an ACS-PRF grant #45214-G7, NSF grant CBET-0736037, and an NSF Career award. We thank the NSF-REU programs at Clemson University (AST-0353849) and Iowa State University (CHE-0453444) for supporting the research of Justin Ching and John Lyons. We are grateful to Professor Prabal Maiti for providing partial charges for the Dreiding model of G3-PAMAM.

REFERENCES

[1] Meijer, E.W.; Van Genderen, M.H.P. *Nature*, **2003**, *426*, 128.
 [2] Bosman, A.W.; Janssen, H.M.; Meijer, E.W. *Chem. Rev.*, **1999**, *99*, 1665.
 [3] Klajnert, B.; Bryszewska, M. *Acta Biochim. Pol.*, **2001**, *48*, 199.
 [4] Sun, L.; Crooks, R.M. *Langmuir*, **2002**, *18*, 8231.

[5] Mynar, J.L.; Lowery, T.L.; Wemmer, D.E.; Pines, A.; Frechet, J.M.J. *J. Am. Chem. Soc.*, **2006**, *128*, 6334.
 [6] Stasko, N.A.; Schoenfish, M.H. *J. Am. Chem. Soc.*, **2006**, *128*, 8265.
 [7] Wang, C.; Wyn-Jones, E.; Sidhu, J.; Tam, K.C. *Langmuir*, **2007**, *23*, 1635.
 [8] Yoo, H.; Juliano, R.L. *Nucleic Acids Res.*, **2000**, *28*, 4225.
 [9] de Groot, F.M.H.; Albrecht, C.; Koekkoek, R.; Beusker, P.H.; Scheeren, H.W. *Angew. Chem. Int. Ed.*, **2003**, *42*, 4490.
 [10] Pan, G.; Lemmouchi, Y.; Akala, E.O.; Bakare, O. *J. Bioact. Compat. Polym.*, **2005**, *20*, 113.
 [11] Froehling, P. *J. Polym. Sci. Part A: Poly Chem.*, **2004**, *42*, 3110.
 [12] Halford, B. *Chem. Eng. News*, **2005**, *83*, 30.
 [13] Helms, B.; Meijer, E.W. *Science*, **2006**, *313*, 929.
 [14] Makogon, Y.F.; Makogon, T.Y.; Holditch, S.A. *Ann. NY Acad. Sci.*, **2000**, *912*, 777.
 [15] Ishijima, A.; Yanagida, T. *Trends Biochem. Sci.*, **2001**, *26*, 438.
 [16] Plimpton, S.J. *J. Comp. Phys.*, **1995**, *117*, 1. <http://lammps.sandia.gov>
 [17] Mayo, S.L.; Olafson, B.D.; Goddard, W.A. *J. Phys. Chem.*, **1990**, *94*, 8897.
 [18] Jorgensen, W.L.; Chandrasekhar, J.; Madura, J.D.; Impey, R.W.; Klein, M.L. *J. Chem. Phys.*, **1983**, *79*, 926.
 [19] Lee, I.; Athey, B.D.; Wetzel, A.W.; Meixner, W.; Baker, J.R. *Macromolecules*, **2002**, *35*, 4510.
 [20] Maiti, P.K.; Cagin, T.; Lin, S.T.; Goddard, W.A. *Macromolecules*, **2005**, *38*, 979.
 [21] Maiti, P.K.; Cagin, T.; Wang, G.; Goddard, W.A. *Macromolecules*, **2004**, *37*, 6236.
 [22] Hockney, R.W.; Eastwood, J.W. *Computer Simulation Using Particles*; Adam Hilger: New York, **1988**.
 [23] Prosa, T.J.; Bauer, B.J.; Amis, E.J.; Tomalia, D.A.; Scherrenberg, R. *J. Polym. Sci. Part B – Polym. Phys.*, **1997**, *35*, 2913.
 [24] Rathgeber, S.; Gast, A.P.; Hedrick, J. L. *Appl. Phys. A – Mater. Sci. Process*, **2002**, *74*, S396.
 [25] Humphrey, W.; Dalke, A.; Schulten, K. *J. Mol. Graph.*, **1996**, *14*, 33.
 [26] Choi, Y.S.; Mecke, A.; Orr, B.G.; Banaszak Holl, M.M.; Baker, J.R. *Nano Lett.*, **2004**, *4*, 391.
 [27] Han, M.; Chen, P.Q.; Yang, X.Z. *Polymer*, **2005**, *46*, 3481.
 [28] Maiti, P.K.; Goddard, W.A. *J. Phys. Chem. B*, **2006**, *110*, 25628.
 [29] Lee, H.; Baker, J.R.; Larson, R.G. *J. Phys. Chem. B*, **2006**, *110*, 4014.
 [30] Opitz, A.W.; Wagner, N.J. *J. Polym. Sci. Part B – Polym. Phys.*, **2006**, *44*, 3062.
 [31] Klajnert, B.; Janiszewska, J.; Urbanczyk-Lipkowska, Z.; Bryszewska, M.; Eband, R.M. *Int. J. Pharm.*, **2006**, *327*, 145.
 [32] Lee, H.; Larson, R.G. *J. Phys. Chem. B*, **2006**, *110*, 18204.
 [33] Pasupathy, K.; Lin, S.; Hu, Q.; Luo, H.; Ke, P.C. *Biotechnol. J.*, **2008**, *3*, 1078.
 [34] Milner, S.T.; McLeish, T.C.B. *Macromolecules*, **1997**, *30*, 2159.
 [35] Freedman, K.O.; Lee, J.; Li, Y.; Luo, D.; Skobeleva, V.B.; Ke, P.C. *J. Phys. Chem. B*, **2005**, *109*, 9839.

Received: September 27, 2008

Revised: October 22, 2008

Accepted: October 23, 2008

© Pasupathy et al.; Licensee Bentham Open.

This is an open access article licensed under the terms of the Creative Commons Attribution Non-Commercial License (<http://creativecommons.org/licenses/by-nc/3.0/>) which permits unrestricted, non-commercial use, distribution and reproduction in any medium, provided the work is properly cited.